HHS Public Access

Author manuscript

Nat Mater. Author manuscript; available in PMC 2020 October 27.

Published in final edited form as:

Nat Mater. 2020 August ; 19(8): 910–920. doi:10.1038/s41563-020-0674-z.

A Year-Long Extended Release Nanoformulated Cabotegravir Prodrug

Tanmay A. Kulkarni[2,†], **Aditya N. Bade**[1,†], **Brady Sillman**[1], **Bhagya Laxmi Dyavar Shetty**[1], **Melinda S. Wojtkiewicz**[1], **Nagsen Gautam**[2], **James R. Hilaire**[1], **Sruthi Sravanam**[1], **Adam Szlachetka**[1], **Benjamin G. Lamberty**[1], **Brenda M. Morsey**[1], **Howard S. Fox**[1], **Yazen Alnouti**[2], **JoEllyn M. McMillan**[1], **R. Lee Mosley**[1], **Jane Meza**[3], **Paul L. Domanico**[4], **Tai-Yuen Yue**[4], **Gary Moore**[4], **Benson J. Edagwa**[1,*], **Howard E. Gendelman**[1,2,*]

[1]Department of Pharmacology and Experimental Neuroscience, University of Nebraska Medical Center, Omaha, NE 68198

[2]Department of Pharmaceutical Sciences, University of Nebraska Medical Center, Omaha, NE 68198

[3]Department of Biostatistics, University of Nebraska Medical Center, Omaha, NE 68198

[4]Department of Global Health Sciences, The Clinton Health Access Initiative, Boston, MA 02127

Abstract

[*]Corresponding authors: Howard E. Gendelman, M.D., Department of Pharmacology and Experimental Neuroscience, University of Nebraska Medical Center, Omaha, NE 68198-5880, USA; phone: 402-559-8920; fax: 402-559-3744; hegendel@unmc.edu, and Benson J. Edagwa, Ph.D., Department of Pharmacology and Experimental Neuroscience, University of Nebraska Medical Center, Omaha, NE 68198-5800, USA; phone: 402-559-8916; fax: 402-559-7495; benson.edagwa@unmc.edu.

[†]Contributed equally

Author contributions

T.A.K.: synthesized the prodrugs, performed the formulation characterization and cell-based laboratory experiments and interpreted the data, prepared the figures, and co-wrote the manuscript; A.N.B.: designed and carried out the laboratory and rodent experiments, analyzed and interpreted the data, supervised the project, prepared the figures and tables, and co-wrote and edited the manuscript; B.S., B.L.D.S., M.S.W., N.G., J.R.H. and S.S.: performed the laboratory, physicochemical and or rodent experiments; A.S. prepared NM2CAB in the Nebraska Nanomedicine Production Plant using GLP protocols; B.G.L., B.M.M., and H.S.F. performed and analyzed the data from the nonhuman primate experiments; P.L.D., T-Y.Y., and G.M. designed and executed the prodrug recrystallization, scale up and formulation manufacture experiments; Y.A.: performed data acquisition and interpretation; J.M.M.: designed, supervised and analyzed the mass spectrometry data; R.L.M and J.M. performed statistical evaluations and data analyses; B.J.E.: was responsible for project conception, study and prodrug design, chemical drug synthesis and nanoformulation schemes, provided supervision, data analyses and interpretation, manuscript editing and provided funding acquisitions; H.E.G.: was responsible for project conception and study integration, integrated each of the study arms, supervised experimental design and data interpretation, co-wrote and edited the manuscript and provided funding acquisitions. All authors critically evaluated the manuscript prior to submission.

Competing interests

B.J.E. and H.E.G. are named inventors on patents that cover the medicinal and polymer chemistry technologies employed in this manuscript encompassing the synthesis of long acting cabotegravir prodrugs and formulation manufacturing. H.E.G. is the Interim Director of the Nebraska Nanomedicine Production Plant, a good manufacturing program facility. The authors declare that this work was produced solely by the authors and that no other individuals or entities influenced any aspects of the work including, but not limited to, the study conception and design, data acquisition, analyses and interpretation, and writing of the manuscript. No other entities provided funds for the work. The authors further declare that they have received no financial compensation from any other third parties for any aspects of the published work. The remaining authors declare no competing interests.

Data availability

The data supporting the study's findings are available within the article and its supplementary files or from the corresponding authors upon request. All the relevant data used to generate Figures 4a, 4c–k, 5a–h, 5i, 6a and 6b–c are included as Source Data.

Long-acting cabotegravir (CAB) extends antiretroviral drug (ARV) administration from daily to monthly. However, dosing volumes, injection site reactions, and health care oversight are obstacles towards broad usage. The creation of poloxamer-coated hydrophobic and lipophilic CAB prodrugs with controlled hydrolysis and tissue penetrance can overcome these obstacles. To such ends, fatty acid ester CAB nanocrystal prodrugs with 14, 18, and 22 added carbon chains were encased in biocompatible surfactants named NMCAB, NM2CAB, and NM3CAB and tested for drug release, activation, cytotoxicity, antiretroviral activities, pharmacokinetics (PK), and biodistribution. PK studies, performed in mice and rhesus macaques, with the lead 18-carbon ester chain NM2CAB, showed plasma CAB levels above the protein-adjusted 90% inhibitory concentration for up to a year. The NM2CAB, compared to NMCAB and NM3CAB, demonstrated prolonged drug release, plasma circulation time and tissue drug concentrations after a single 45 mg/kg intramuscular injection. These prodrug modifications could significantly improve CAB's effectiveness.

Current antiretroviral drug (ARV) regimens are potent and well-tolerated, enabling sustained, life-long suppression of human immunodeficiency virus type one (HIV-1) infection[1]. However viral control is linked to regimen adherence affected by disease co-morbidity, stigma, behavior, illicit drug-use, and cost[1]. Such limitations were the impetus towards the development of long-acting (LA) injectables[2,3, 4, 5, 6]. In April, 2019, ViiV Healthcare submitted a New Drug Application to the US Food and Drug Administration (FDA) for monthly cabotegravir and rilpivirine (CAB and RPV) injectables applied in HIV-1 treatments[7]. While approval was initially denied, the complete response letter received in December 2019[8] focused on Chemistry Manufacturing and Controls not product safety[8]. Nonetheless, considerable sustained promise for broad clinical use remain for LA injectables. The "Antiretroviral Therapy as Long-Acting Suppression" and "First Long-Acting Injectable Regimen" studies show safety, efficacy, and drug tolerability[3, 5, 6] as do drug implants[9, 10, 11, 12]. However, notable limitations in both include injection site reactions, large injection volumes, frequent dosing, required health care services, and limited viral tissue reservoir penetrance[4, 13, 14]. Thus, immediate improvements in LA ARV regimens are needed for use in pre-exposure prophylaxis (PrEP), HIV-1 transmission control, and for maintenance therapy in virologically suppressed patients placed first on other ARV regimens.

To such ends, LA ARV prodrug libraries were created from lipophilic fatty esters to optimize drug release and prodrug hydrolysis rates resulting in sustained therapeutic native drug levels in plasma and tissue[14, 15, 16, 17, 18, 19]. Despite such improvements, there remains no defined pathways to optimize prodrug hydrolysis rates and other physicochemical features. To this end, we now report the synthesis and physiochemical characterization of variable 14, 18, and 22 carbon ester-modified CAB (MCAB, M2CAB, and M3CAB) and their respective nanoformulations (NMCAB, NM2CAB, and NM3CAB). The lead 18 carbon ester NM2CAB enhanced human macrophage drug uptake and retention with sustained protection against HIV-1 challenge. NM2CAB generated CAB plasma concentrations above the protein-adjusted 90% inhibitory concentration (PA-IC_{90}) of 166 ng/mL for up to one year with detectable lymphoid, mucosal, and gut biodistribution after a single 45 mg/kg parenteral dose with no recorded adverse events in animal models. We posit

that optimizing CAB prodrug features could improve native CAB effectiveness and based on such an extended apparent half-life could create the potential for a vaccine mimetic.

Creation and characterization of CAB prodrugs

CAB was chemically modified by attaching fatty acid esters of variable carbon lengths (C14, C18, and C22) to produce MCAB, M2CAB, and M3CAB prodrugs (Figure 1a).

Each was characterized by nuclear magnetic resonance (NMR), Fourier Transform Infrared spectroscopy (FTIR), electrospray ionization mass spectrometry (ESI-MS), and X- ray powder diffraction (XRD) to confirm chemical structures and purity (Figure 1b, Supplementary figures 1–4, and Supplementary table 1). Significant reductions in the aqueous solubility of MCAB (0.13 ± 0.03 μg/mL), M2CAB (0.10 ± 0.03 μg/mL) and M3CAB (0.04 μg/mL) compared to CAB (34.31 ± 4.8 μg/mL) were recorded (Figure 1c). The LogP values for MCAB, M2CAB, and M3CAB were 4.56, 4.89, and 5.12, respectively, compared to 0.16 for CAB (Supplementary table 1). These results confirmed enhanced prodrug hydrophobicity and lipophilicity.

Pharmacologically inactive prodrugs require enzymatic or hydrolytic activation in physiological conditions for active drug bioconversion[20, 21]. Therefore, hydrolysis kinetics of MCAB, M2CAB, and M3CAB and subsequent CAB formation were evaluated in mouse, rat, rabbit, monkey, dog, and human plasma demonstrating > 85% cleavage of MCAB in 30 minutes. M2CAB showed an average 75 and 80% cleavage within 2 and 6 hours. M3CAB showed 50% prodrug cleavage after 24 hours (Figure 1e). Differences in prodrug hydrolysis paralleled divergent species-specific plasma esterase activities[22]. Next, the half-maximal effective concentrations (EC_{50}) of MCAB, M2CAB, and M3CAB were tested. HIV-1 reverse transcriptase (RT) activities in the culture medium of monocyte-derived macrophages (MDM) infected with HIV-1_{ADA} demonstrated comparable EC_{50} values, indicating that the modifications did not affect drug antiviral activities (Figure 1d).

Manufacturing and long-term formulation stability

Scalable nanocrystal manufacture techniques[23, 24] were employed to generate nanoformulations of CAB (NCAB), MCAB (NMCAB), M2CAB (NM2CAB), and M3CAB (NM3CAB) by high-pressure homogenization. Drug loading for CAB and M2CAB was > 80% with < 1% of uncoated prodrug in the NM2CAB nanocrystals, using poloxamer 407 (P407) as the stabilizer in water (Supplementary table 2). Scanning electron microscopy (SEM) images showed uniform rod-shaped nanoparticle morphologies (Figure 2a). Nanoparticle sizes, polydispersity indices (PDI), and zeta potentials were determined as measures of stability by dynamic light scattering (DLS) at room temperature, 4 °C, and 37 °C (Figure 2b). The particle sizes and PDIs remained narrow over 98 days indicating minimal aggregation. Zeta potentials of −25 to −35 mV indicated high particle stability through electrostatic repulsion. All formulations remained stable up to 98 days, signifying that the nanosuspensions maintain their integrity under a range of storage conditions reflective of need in resource-limited settings (Figure 2b). Reproducibility was confirmed in

11 separate NM2CAB batches (Supplementary table 3). Nanoparticle sizes varied from 243 ± 2 nm to 378 ± 1 nm with a narrow PDI (0.18 to 0.33).

Nanoformulations' effects on prodrugs antiretroviral activity (EC_{50}) were determined in MDM (Supplementary figure 5). EC_{50} values were increased compared to non-nanoformulated drug or prodrugs. Required nanoparticles dissolution, prior to cleavage of prodrugs, could account for the increased EC_{50} values and were comparable for NCAB (39.83 nM), NMCAB (89.67 nM), and NM2CAB (37.02 nM). However, the EC_{50} value for NM3CAB increased (~1.78×10^6 nM), which could be linked to slower prodrug conversion to active CAB (Figure 1e). Cellular vitality was assessed in MDM using the 3-(4,5-dimethylthiazol-2-yl)-2,5-diphenyltetrazolium bromide (MTT) assay (Supplementary figure 6). No formulation-induced cytotoxicity was seen at 10 to 400 μM drug or prodrug concentrations.

MDM uptake, retention, release, and antiretroviral efficacy

The phagocytic and tissue migratory macrophage functions enable its use as cellular drug depots and carriers[14, 25, 26, 27]. Therefore, laboratory macrophage modeling was used to assess uptake, retention, release, and antiretroviral activities of nanoformulated ARV prodrugs[14, 16, 17, 18, 19]. Formulation uptake was assessed in MDM by measuring drug and prodrug levels after 100 μM treatment with NCAB, NMCAB, NM2CAB, or NM3CAB over 24 hours (Figure 3a). Intracellular prodrug levels for NMCAB, NM2CAB, and NM3CAB were 61.69 ± 0.78, 84.07 ± 5.82, and 73.34 ± 13.59 nmol/10^6 cells, respectively at 24 hours; and intracellular CAB levels were 0.58 ± 0.11, 12.31 ± 0.46, 17.79 ± 2.92, and 7.97 ± 1.76 nmol/10^6 cells for NCAB, NMCAB, NM2CAB, or NM3CAB, respectively (Figure 3a). Following treatment with 100 μM of each nanoformulation for 8 hours, we evaluated the ability of macrophages to retain intracellular drug and prodrugs over a period of 30 days (Figure 3b). Intracellular prodrug levels were sustained for 30 days at 0.41 ± 0.09, 14.21 ± 2.28, and 26.70 ± 3.29 nmol/10^6 cells for NMCAB, NM2CAB, and NM3CAB, respectively (Figure 3b). Similarly, intracellular CAB levels formed from prodrug cleavage for NM2CAB and NM3CAB were 1.71 ± 0.35 and 2.05 ± 0.10 nmol/10^6 cells at day 30. NMCAB treatment showed CAB levels at the detection limit at day 25. CAB levels fell below the limit of quantitation after one day of NCAB treatment (Figure 3b). CAB released from these cells into culture medium was also measured. NM2CAB provided the most sustained CAB release with medium drug concentrations of 1.98 ± 0.18 nmol/mL at day 10 and 1.0 ± 0.10 nmol/mL at day 30. CAB release from NMCAB treated cells was rapid with concentrations of 16.29 ± 0.84 nmol/mL at day 10 and 3.19 ± 1.46 nmol/mL at day 30. CAB was not detected in culture medium with NCAB and NM3CAB treatments after 5 and 10 days, respectively (Figure 3c). Prodrugs were not detected in culture medium for any of the treatments. Transmission electron microscopy (TEM) images of MDM confirmed the presence of prodrug nanoformulations (NM2CAB and NM3CAB) in cytoplasmic vesicles further signifying a macrophage drug depot (Figure 3d). To determine whether sustained drug retention in MDM would protect against HIV-1 infection, we challenged cells with HIV-1_{ADA} for up to 30 days following treatment with 100 μM NCAB, NMCAB, or NM2CAB. NM3CAB was not selected for this study as it did not show protection at the desired EC_{50} value (Supplementary figure 5). NM2CAB treatment suppressed HIV-1 RT

activity (Figure 3e) and was confirmed by the absence of HIV-1 p24 expression up to day 30 (Figure 3f). In contrast, complete viral breakthrough occurred at day 1 after NCAB and day 20 after NMCAB treatment. NM2CAB provided a “best” protection against HIV-1 challenge. In addition, 10, 50, or 100 μM NM2CAB treatment induced sustained antiretroviral activity (Figure 3g and h). Complete viral suppression was observed with 50 and 100 μM NM2CAB treatments, while 10 μM treatment provided 57% protection after 30 days (Figure 3g); results were validated by HIV-1 p24 expression (Figure 3h).

Year-long plasma CAB levels after a single NM2CAB injection

To assess pharmacokinetic (PK) and biodistribution (BD) profiles, female NSG (NOD scid gamma) mice were injected intramuscularly (IM) with a single dose of 45 mg/kg CAB-equivalents of NCAB, NMCAB, or NM2CAB. NCAB reflects US FDA filed CAB LA and thus was used as a control (Supplementary figure 7). At day 1 after NCAB treatment, higher plasma CAB concentrations were detected compared to both NMCAB and NM2CAB. However, NCAB showed faster decay compared to NM2CAB (Figure 4). For NCAB treatment, plasma CAB concentrations were above 4×PA-IC_{90} (664 ng/mL) up to day 35 (792.7 ng/mL), then rapidly declined to below the PA-IC_{90} (166 ng/mL) by day 49 (75 ng/mL). At day 126, CAB values were below the limit of detection (0.5 ng/mL). NMCAB treatment showed slower CAB decay, and CAB levels were maintained above 4×PA-IC_{90} up to day 91 (673.8 ng/mL) and above the PA-IC_{90} at 186.7 ng/mL at day 168. At day 364 after NMCAB treatment, CAB levels were 8.5 ng/mL. NM2CAB demonstrated slower plasma CAB decay compared to both NCAB and NMCAB for the entire study, maintaining sustained plasma CAB levels above the 4×PA-IC_{90} at 702.0 ng/mL at day 231 and above the PA-IC_{90} at 354 ng/mL at day 364. PK parameters were determined using noncompartmental analysis for all treatment groups (Figure 4b). The apparent CAB half-life ($t_{0.5}$) following NM2CAB (131 days) treatment was 17- and 3-fold longer than NCAB (7 days) and NMCAB (44 days), respectively. Similarly, CAB mean residence time (MRT) for NM2CAB (201 days) was 21-fold longer than NCAB (9 days) and 7-fold longer than NMCAB (30 days). NM2CAB elicited higher CAB tissue levels than NMCAB and NCAB treatments (Figure 4c–k). At day 28, CAB tissue levels were comparable between NCAB and NM2CAB. However, by day 42, CAB tissue levels after NCAB treatment were lower than those observed for NM2CAB (vagina, spleen, gut, liver, lymph node, kidney, lung, rectum, and brain). CAB levels in tissues, up to day 42 following NMCAB treatment, were significantly higher than NCAB and NM2CAB. However, at day 364, CAB concentrations were readily found in tissues in the NM2CAB treated group. Here, CAB levels were 32.5, 19.6, 49.7, and 67.6 ng/g in vagina, rectum, spleen, and lymph nodes; and 104.4, 12.3, 8.3, 36.0, and 35.5 ng/g in liver, gut, brain, kidney, and lung (Figure 4c–k). MCAB and M2CAB prodrug concentrations were also quantified in blood and tissues (Figure 5). At day 1 after injection, MCAB and M2CAB concentrations in blood were 22 and 31.3 ng/mL, respectively, and rapidly declined below the limit of detection thereafter (Figure 5i). All screened tissues were prodrug depots (Figure 5a–h). Notably, MCAB levels were significantly lower than M2CAB levels at days 14, 28, and 42, and were undetectable by day 364. For NM2CAB, at day 364, prodrug levels were 2973.3, 958.4, 38.5, 50.3, 4.2, and 18710.1 ng/g in spleen, liver, lung, brain, kidney, and lymph nodes, respectively. Next, a

single IM injection of NM3CAB (45 mg/kg CAB-equivalents) in female NSG mice generated lower levels of plasma CAB (2248 ng/mL) at day 1 compared to 41237.6, 30148.9, and 7076.1 ng/mL for NCAB, NMCAB, and NM2CAB, respectively (Supplementary figure 8). Plasma CAB levels were around the PA-IC_{90} (233.2 ng/mL) within 28 days after treatment. In addition, CAB levels in tissues (spleen, liver, brain, gut, and lymph nodes) reflected low plasma CAB concentrations at day 28 (Supplementary figure 8). Slower hydrolysis of M3CAB was validated in BALB/cJ mice (Supplementary figure 9). Similar to PK results in NSG mice, NM3CAB treatment generated low levels of plasma CAB that fell below the PA-IC_{90} by 28 days with values of 98.8 ng/mL. These data confirmed an impeded hydrolysis of M3CAB to CAB. Therefore, since our objective is to develop a formulation with six months or longer dosing interval, the NM3CAB treatment group was terminated from further evaluation.

Superior PK and BD profiles of NM2CAB among all formulations were confirmed in BALB/cJ mice. Normal mice were used to validate the results from immunodeficient NSG mice. PK and BD assessments in plasma and tissues for NM2CAB paralleled those in NSG mice (Supplementary figure 10). Plasma CAB concentrations of 170.8 ng/mL were above the PA-IC_{90} at day 231. In contrast, CAB plasma levels following NCAB treatment fell below the PA-IC_{90} to 12.3 ng/mL at day 28. To validate the results seen in mice, rhesus macaques (RM) were injected IM with single dose of 45 mg/kg CAB-equivalents of NM2CAB (Figure 6). Plasma CAB and M2CAB prodrug levels were measured up to day 365. Similar to results in mice, NM2CAB treatment provided slow plasma CAB decay kinetics, maintaining plasma CAB concentrations for up to 364 days. CAB levels were measured at an average of 66.9 ng/mL at day 365. As observed in mice, plasma M2CAB concentrations were lower throughout the study compared to CAB levels (Figure 6a). At day 204 following NM2CAB administration, CAB concentrations in rectal, lymph nodes, and adipose tissues were 10.1, 21.9, and 29.5 ng/g, respectively (Figure 6b). M2CAB was present at higher levels in lymph node and adipose tissues (33.3 and 233.2 ng/g) with lower levels (1.7 ng/g) in rectal tissue (Figure 6c). Statistical analysis determined that assessment in MDM directly correlated with PK measurements (Supplementary table 4).

Toxicity assessments

Toxicity was assessed in mice and RM following NM2CAB treatment. For NSG mice, animal weights were recorded weekly for one year; at the study conclusion (day 364), plasma and tissues were collected for metabolic profiles and histopathology, respectively (Supplementary figure 11). Controls were age matched untreated mice. No differences in weights were observed between the control and treatment groups (Supplementary figure 11a). Comprehensive serum chemistry profiles were quantified; no significant differences were noted between controls and NM2CAB treated groups (Supplementary figure 11b) indicating that NM2CAB did not adversely affect functions of systemic organs. Hematoxylin and eosin (H&E)-stained tissue sections, examined by a certified pathologist, revealed no abnormal pathology in NM2CAB treated animals (Supplementary figure 11c). For assessment in RM, weights were recorded, and complete blood counts and metabolic profiles were assessed for up to 365 days after NM2CAB dosing (Figure 6d and 6e). No changes in any animals' weights were observed (Supplementary figure 12). An initial mild

redness observed at the site of injection was resolved by day 3 in all animals. Total white cell, neutrophil, lymphocyte, and monocyte counts were unchanged during the study period (Figure 6d). At day 1 after injection, increased neutrophil counts were observed, which then resolved to normal within 2 weeks for all animals. Such a change could be related to the injection itself and not be drug-associated[28]. Liver and kidney metabolic profiles were unchanged in all animals following treatment (Figure 6e). Overall, no adverse events were observed after NM2CAB administration.

ARV prodrug drug-drug interactions

We evaluated the potential of drug-drug interactions between NM2CAB and a best performing RPV prodrug nanoformulation (NM3RPV). RPV was chosen along with CAB based on the current clinical development of long-acting CAB and RPV formulations for combination treatment[3, 4, 5, 6]. NM3RPV is a long-acting prodrug formulation of RPV developed by our laboratory[16]. BALB/cJ male mice were treated IM with a single dose of NM2CAB alone, NM3RPV alone, or co-administration of NM2CAB and NM3RPV. No differences in plasma CAB and RPV concentrations were observed between animals treated with single or combined drug formulations (Supplementary figure 13).

Formulation scalability

Considering the need for bench-to-bedside translation, we examined NM2CAB's scalability. First, we recrystallized then produced NM2CAB at high prodrug concentrations. Recrystallization provides purity control and is broadly used by the pharmaceutical industry[29]. For NM2CAB recrystallization, the solvents tested were acetonitrile (ACN), methyltetrahydrofuran (MeTHF), cyclopentyl methyl ether (CPME) and toluene (PhMe). Recovery yields, melting points, and purity were determined (Supplementary table 5). M2CAB yields were highest for ACN (70%) and CPME (85%). Recovery was temperature and solubility dependent. The melting point was narrow after recrystallization for all solvents. A modest increase in the melting point was observed for ACN solids (123–125 °C) compared to original sample (116–122 °C). The purity profiles of M2CAB before and after recrystallization from ACN and CPME were equivalent (Supplementary table 5). The XRD assessment of physical appearances of the solids from ACN and CPME were similar to the original M2CAB (Supplementary figure 14). Next, the manufacturing scheme for scale-up production of NM2CAB at high concentrations was evaluated. Stable NM2CAB was manufactured at 400 mg/mL drug concentration under good laboratory practices (GLP). Thus, < 1 mL of NM2CAB injection volume would be required in patients when extrapolated from current dosing[30].

Discussion

LA ARVs suppress viral replication equally to oral medicines while affecting regimen adherence[4, 5, 6, 31, 32, 33]. The development of LA slow effective release antiretroviral therapy (LASER ART) formulations by our laboratories have given additional promise to the first phase of LA regimens[34]. Herein, a single injection of NM2CAB generated substantial improvements in drug PK, reflected by sustained plasma drug concentrations and tissue BD

compared to NCAB, NMCAB, or NM3CAB. NM2CAB provided extended plasma CAB decay in mice and RM while maintaining drug levels above the PA-IC_{90} of 166 ng/mL for one year following a single injection. In all, an approximate 20-fold improvement in PK parameters was seen compared to the first-generation CAB LA. The variability in plasma CAB concentrations among the tested strains and species could be a result of differences in body fat distribution, muscle mass, physical activity, and carboxylesterases enzymes required for prodrug hydrolysis[22, 35, 36]. CAB LA was studied extensively in RM. These studies demonstrated that CAB LA provided a high degree of protection against vaginal, rectal, parenteral, and penile challenges with simian-HIV (SHIV) strains, affirming its future use as PrEP for people at high risk for sexual HIV-1 exposure and for intravenous drug users[37, 38]. Plasma levels above 3×PA-IC_{90} provided 100% protection, and concentrations above the PA-IC_{90} provided 97% protection against viral challenge. Herein, NM2CAB administration generated plasma CAB concentrations above PA-IC_{90} for up to a year, signifying its potential use for PrEP. Moreover, there are several advantages of NM2CAB over investigational CAB LA. *First*, manufacturing of NM2CAB at a concentration of 400 mg/mL, which is twice the 200 mg/mL for CAB LA. *Second*, NM2CAB would require < 1 mL injection volume for a yearly administration rather than 2 mL injection volume of CAB LA for a monthly dosing. Thus, NM2CAB can overcome major obstacles of CAB LA: dosing volume, administration intervals, and injection site reactions.

The discoveries made in this report demonstrate a “sweet spot” in prodrug product profiles enabling a significant extension in CAB’s apparent half-life, safety of administration, and ease of manufacture for immediate global PrEP. The innovative molecular design of prodrug not only provided favorable physicochemical properties but also resulted in a crystalline and thermally stable compound facilitating its successful manufacture. Importantly, like approaches can affect improved pharmacokinetic and targeting properties of medicines used to treat a spectrum of infectious, inflammatory, metabolic, and/or degenerative disorders[39].

Nonetheless, long-acting CAB formulations can meet the challenge of therapeutic regimen adherence in broad patient groups that include children, adolescents and pregnant and postpartum women[4,37, 38]. While Phase 2 and Phase 3 LA ARV clinical trials are encouraging[5, 6, 13, 40, 41] limitations are acknowledged that include requirements for an oral lead-in for safety. Moreover, a prolonged pharmacologic tail after discontinuation could result in drug resistant viral strains as reported for RPV LA[42]. The lack of activity against major co-infections such as hepatitis B virus (HBV)[43] and potential drug-drug interactions are other considerations. For example, combined use of CAB and rifampin could reduce CAB exposure. Individuals receiving such a once-a-year CAB and diagnosed with tuberculosis would be cautioned against the use of rifampin. Here rifabutin would be an alternative[44, 45].

Taken together, CAB prodrugs chemically modified with 14, 18, or 22 carbon chain esters encased into surfactant-coated nanoformulations were created. Evaluations of prodrug hydrolysis and PK profiles demonstrated that NM2CAB produced a “once-a-year” injectable profile. Particularly, in the absence of protective vaccines against HIV-1[46, 47], effective long-acting ART not only are the best approaches for PrEP[47] but also could serve as a vaccine-mimetic if dosing intervals are extended to yearly or longer. Moreover, CAB’s activities

against HIV-2 provides real potential for dual treatment[48, 49]. Altogether, we conclude that a major extension of the dosing interval could allow NM2CAB to be developed as a vaccine-mimetic.

Methods

Reagents

CAB was purchased from BOC Sciences (Shirley, NY). Pyridine, dimethylformamide (DMF), N,N-diisopropylethylamine (DIEA), myristoyl chloride, stearoyl chloride, behenic acid, pluronic F127 (poloxamer 407; P407), PEG 3350, ciprofloxacin, 3-(4,5-dimethylthiazol-2-yl)-2,5-diphenyltetrazolium bromide (MTT), dimethyl sulfoxide (DMSO), paraformaldehyde (PFA), and 3,3'-diaminobenzidine (DAB) were purchased from Sigma-Aldrich (St. Louis, MO). Diethyl ether, ethyl acetate, hexanes, acetonitrile (ACN), methanol, MS-grade water, cell culture grade water (endotoxin-free), gentamicin, potassium phosphate monobasic (KH_2PO_4), bovine serum albumin (BSA), Triton X-100, and TRIzol reagent were purchased from Fisher Scientific (Hampton, NH). Monoclonal mouse anti-human HIV-1 p24 (clone Kal-1) and polymer-based HRP-conjugated anti-mouse EnVision+ secondary were purchased from Dako (Carpinteria, CA). Heat-inactivated pooled human serum was purchased from Innovative Biologics (Herndon, VA). Dulbecco's Modified Eagle's Medium (DMEM) was purchased from Corning Life Sciences (Tewksbury, MA).

Synthesis and characterization of CAB prodrugs

A series of three prodrugs were synthesized by esterification of the hydroxyl group on CAB yielding lipophilic prodrugs with 14, 18, and 22 carbon chains and were named MCAB, M2CAB, and M3CAB, respectively. Specifically, CAB was dried from anhydrous pyridine and then suspended in anhydrous DMF. The mixture was cooled to 0 °C under argon. DIEA (2 equivalents) was used to deprotonate the hydroxyl group of CAB and then reacted with 2 equivalents myristoyl- and stearoyl- chloride for 24 hours to obtain MCAB and M2CAB, respectively. M3CAB was synthesized in a two-step process. First, behenyl chloride was synthesized by reacting one equivalent of behenic acid with four equivalents of thionyl chloride in anhydrous chloroform. The formed acyl chloride was then covalently linked to CAB in the second step to form the M3CAB prodrug. All resultant prodrugs were purified by silica gel column chromatography using an eluent of 4:1 then 9:1 mixture of ethyl acetate and hexanes. The desired compound fractions from the columns were dried on a rotary evaporator, precipitated from diethyl ether to obtain white powders that were further dried under high vacuum to give average chemical yields of 85–95%. Successful synthesis of prodrugs was confirmed by proton and carbon nuclear magnetic resonance (^1H and ^{13}C NMR) spectroscopy using Bruker Avance-III HD (Billerica, MA) operating at 500 MHz, a magnetic field strength of 11.7 T. FTIR was performed on a IR-Prestige 21 (Shimadzu, Columbia, MD). Comparative crystallographic analyses of CAB and prodrugs by XRD were carried out in the 2θ range of 2–70° at a rate of 1°/s using PANalytical Empyrean diffractometer (PANalytical Inc., Westborough, MA) with Cu-Kα radiation (1.5418 Å) at 40 kV, 45 mA setting. Molecular mass was determined by direct infusion into a TQD mass spectrometer.

UPLC-ultraviolet/visible (UV/Vis) quantification of CAB, MCAB, M2CAB, and M3CAB

A Waters ACQUITY ultra-performance liquid chromatography (UPLC) H-Class system with TUV detector and Empower 3 software (Milford, MA) was used to measure drug concentrations. CAB, MCAB, M2CAB, and M3CAB samples were separated on a Phenomenex Kinetex 5 μm C18 column (150 × 4.6 mm) (Torrance, CA). CAB was detected at 254 nm, using an isocratic elution with a mobile phase consisting of 65% 50 mM KH2PO4, (pH 3.2), and 35% ACN and a flow rate of 1.0 mL/minute. MCAB, M2CAB, and M3CAB were detected at 230 nm, using a gradient elution starting with a mobile phase consisting of 90% ACN/10% water, to 95% ACN/5% water, and finally to 98% ACN/2% water at a flow rate of 1.0 mL/minute. Drug content was determined relative to peak areas of drug standards (0.05–50 μg/mL) in methanol.

Solubility

The LogP, aqueous solubility, and 1-octanol solubility of CAB, MCAB, M2CAB, and M3CAB were determined by adding drug to a mixture of water and 1-octanol at room temperature then mixing for 48 hours. Samples were centrifuged at 20,000 × g for 10 minutes to pellet insoluble drug. Aqueous supernatants were frozen, lyophilized then resuspended in methanol (MeOH). 1-octanol supernatants were prepared for analysis by dilution in MeOH and samples analyzed for drug content by UPLC.

Plasma prodrug cleavage kinetics

The hydrolysis kinetics of MCAB, M2CAB, and M3CAB and release of the active drug were determined in plasma of different species (mouse, rat, rabbit, monkey, dog, and human). MCAB, M2CAB, or M3CAB (1 μM) were incubated in 100 μL plasma at 37 °C. At specified time points, 1 mL methanol buffer (0.1% formic acid; 25 mM ammonium formate) was added to each sample and vortexed for 3 minutes to stop the reaction. For the 0-minute time-point, 100 μL ice cold plasma was spiked with 1 μM of each prodrug, and 1 mL of ice cold methanol buffer was added immediately. Following the addition of MeOH, samples were centrifuged at 15,000 × g for 10 minutes, and the supernatants were analyzed for drug content by UPLC-MS/MS (Waters Xevo TQ-XS).

Nanoparticle synthesis and characterization

Nanoformulations of CAB (NCAB) and prodrugs (NMCAB, NM2CAB, and NM3CAB) were manufactured by high-pressure homogenization using the surfactant P407. Briefly, each solid drug/prodrug was dispersed in a P407 solution in endotoxin free water and allowed to form a presuspension. The drug/prodrug to surfactant ratio was maintained at 10:1 (w/w), and a suspension concentration was in the range of 2%−20% w/v of drug/prodrug and 0.2–2% w/v for P407. The presuspension was homogenized on an Avestin EmulsiFlex-C3 high-pressure homogenizer (Ottawa, ON, Canada) at ~18,000 psi until the desired particle size was achieved. Nanoparticles were characterized for particle size (D_{eff}), PDI, and zeta potential by DLS using a Malvern Zetasizer Nano-ZS (Worcestershire, UK). The stabilities of the nanoformulations were monitored at 4 °C, room temperature, and 37°C for 3 months. Drug/prodrug concentration in each nanoformulation was determined by dissolving the nanoformulation in MeOH(1000–10,000 fold dilution) which was then

analyzed by UPLC-UV/Vis. Encapsulation efficiency was calculated using the following equation: encapsulation efficiency (%) = (weight of drug in formulation/initial weight of drug added) x 100. Drug loading was calculated using the following equation: drug loading (%) = (weight of drug in formulation/weight of lyophilized formulation) x 100. For quantitation of uncoated drug in nanosuspensions, homogenized drug formulations (NCAB and NM2CAB) were centrifuged at 20,000 × g for 10 minutes to pellet nanoformulated drug. Supernatants were frozen, lyophilized, and subsequently resuspended in MeOH for analyses. Collected samples were analyzed for drug content by UPLC-UV/Vis as previously described. Nanoparticle morphologies were assessed by SEM. Nanoparticles were fixed in a solution of 2% glutaraldehyde, 2% PFA in 0.1 M Sorenson's phosphate buffer (pH 7.2) at 4 °C for 24 hours, and processed for imaging. Nanosuspensions were air dried onto a glass coverslip mounted on an SEM sample stub and sputter coated with approximately 50 nm of gold/palladium alloy. Samples were assayed using a FEI Quanta 200 scanning electron microscope (Hillsboro, OR) operated at 5.0 kV[17].

Human monocyte-derived macrophages (MDM)

Human monocytes were obtained by leukapheresis from HIV-1/2 and hepatitis B seronegative donors and purified by counter-current centrifugal elutriation. Monocytes were cultured in DMEM containing 4.5 g/L glucose, L-glutamine, and sodium pyruvate supplemented with 10% heat-inactivated human serum, 50 μg/mL gentamicin, and 10 μg/mL ciprofloxacin. Cells were maintained at 37 °C in a 5% CO_2 incubator. Recombinant human macrophage colony stimulating factor (MCSF, 1000 U/mL) was added to the culture media for the first 7 days to facilitate monocyte differentiation into MDMs. Half-culture media was replaced with fresh media every other day. After differentiation, MDM were used for the *in vitro* assays.

Cytotoxicity

Cell viability following treatment with nanoparticles was evaluated using the MTT assay. Human MDM plated in 96-well plates at a density of 0.08×10^6 cells per well were treated with 10, 25, 50, 100, 200, or 400 μM NCAB, NMCAB, NM2CAB, or NM3CAB for 24 hours. Untreated cells were used as controls. For each group, quadruplicate samples were used. Cells were washed with phosphate buffered saline (PBS) and incubated with 100 μL/well of MTT solution (5 mg/mL) for 45 minutes at 37 °C. After incubation, the MTT solution was removed, and cells were washed with PBS. Next, DMSO (200 μL) was added to each well, and the absorbance was measured at 490 nm on a Molecular Devices SpectraMax M3 plate reader with SoftMax Pro 6.2 software (Sunnyvale, CA). Absorbance was compared to that of control cells to determine cytotoxicity.

Drug particle uptake, retention and release

Human MDM were used for *in vitro* assessments. MDM uptake and retention studies were performed in flat-bottom, 12-well plates at a density of 1×10^6 cells/well, with each treatment completed in triplicate. For cellular uptake studies, MDM were treated with 100 μM NCAB, NMCAB, NM2CAB, or NM3CAB. At 2, 4, 8, and 24 hours following treatment, medium was removed; MDM were washed twice with PBS then scraped into 1 mL PBS and counted (Invitrogen Countess Automated Cell Counter, Carlsbad, CA). Cells

were pelleted by centrifugation at 950 × g for 8 minutes at 4 °C. Cell pellets were re-suspended in 200 μL HPLC-grade methanol and sonicated using a probe sonicator to release intracellular drug and prodrug. For retention studies, MDM were treated with 100 μM NCAB, NMCAB, NM2CAB, or NM3CAB for 8 hours, and then washed twice with PBS. Fresh culture medium without drug was added, and half-media volume was replaced every other day. MDM were collected at days 1, 5, 10, 15, 20, 25, and 30, and then processed as described for uptake studies to assay intracellular drug and prodrug concentrations. For both studies, the resultant lysates were centrifuged at 20,000 × g for 10 minutes at 4 °C to separate cell debris from drug containing supernatant. Samples were analyzed for drug and prodrug content by UPLC-UV/Vis. For release studies, culture medium at time points similar to those in the retention study was collected for quantitating the drug and prodrug released by MDM. The culture medium (400 μL) was mixed with MeOH (1 mL) to precipitate proteins and then centrifuged at 17,000 × g for 10 minutes at 4 °C to pellet the non-soluble precipitate. The supernatant was transferred to new tubes and dried using a SpeedVac (ThermoFisher Scientific, Asheville, NC). The dried contents were re-suspended in MeOH and analyzed by UPLC-UV/Vis.

Intracellular particle distribution

MDM were treated with 100 μM NCAB, NMCAB, NM2CAB, or NM3CAB for 8 hours, then washed twice with PBS. Fresh culture medium without drug was added, and half-media volume was replaced every other day. MDM were collected at days 0, 15, and 30 after treatment and analyzed by TEM to image intracellular nanoparticles. For day 0, cells were collected immediately after the 8-hour treatment. At stated time points, cells were washed twice with PBS, scraped into PBS, pelleted at 950 × g for 8 minutes at room temperature, and fixed in a solution of 2% glutaraldehyde, 2% PFA in 0.1 M Sorenson's phosphate buffer (pH 6.2). The fixed cell suspension was placed on a formvar/silicon monoxide 200 mesh copper grid and allowed to settle for 2 minutes. Excess solution was wicked off, and samples were allowed to dry. NanoVan vanadium negative stain was placed on the grid for 1 minute, then wicked away and allowed to dry. Grids were examined on a FEI Tecnai G2 Spirit TWIN transmission electron microscope operated at 80 kV. Images were acquired digitally with an AMT digital imaging system (Woburn, MA)[17].

HIV-1 MDM infection

MDM were plated in flat-bottom 24-well plates at a density of 0.8×10^6 cells/well. MDM were treated with 100 μM NCAB, NMCAB, NM2CAB, or NM3CAB for 8 hours. Following treatment, cells were washed twice with PBS and cultured in fresh culture medium without drug with half-media replacement every other day. At 1, 5, 10, 15, 20, 25, and 30 days after the treatment, the cells were infected with HIV-1_{ADA} at a multiplicity of infection (MOI) of 0.1 infectious particles per cell for 16 hours. Following infection, MDM were washed twice with PBS and replenished with fresh media without virus or drug. Cells were cultured for an additional ten days with half-media replacement every other day and full medium replacement on the 8^{th} day. The culture medium was collected on the 10^{th} day after infection for measurement of HIV-1 RT activity. The extent of infection was determined as the percent of RT activity relative to infected untreated MDM. Cells were fixed in 2% PFA at each time point, and expression of HIV-1 p24 antigen was determined by immunocytochemistry.

Half-maximum effective concentration (EC_{50}) test

MDM were plated in flat-bottom 96-well plates (0.08×10^6 cells/well). Cells were treated with a range of drug concentrations, 0.01–1000 nM, of CAB, MCAB, M2CAB, M3CAB, NCAB, NMCAB, NM2CAB, or NM3CAB for 1 hour prior to infection with HIV-1_{ADA} (MOI of 0.1) for 4 hours. After 4 hours of viral challenge, cells were washed with PBS and given fresh media containing the same concentrations of drug (0.01–1000 nM). Cell supernatants were collected 10 days later and assayed for HIV-1 RT activity as described above.

PK, BD, and drug-drug interaction studies

NSG mice (female, 6–8 weeks, Jackson Labs, Bar Harbor, ME) were administered 45 mg/kg CAB-equivalents of NCAB, NMCAB, NM2CAB, or NM3CAB by a single IM (caudal thigh muscle) injection at 40 μL/25 g mouse. Following injection, blood samples were collected into heparinized tubes at day 1 post-administration and then weekly up to day 364 by cheek puncture (submandibular vein) using a 5 mm lancet (MEDIpoint, Inc., Mineola, NY). Collected blood (25 μL) was immediately diluted into 1 mL ACN for drug measurements. Remaining blood samples were centrifuged at 2,000 × g for 8 minutes for plasma collection and quantitation of plasma drug contents. At days 14, 28, 42, and 364 following administration, animals were humanely euthanized; and spleen, lymph nodes, liver, lung, gut (duodenum/jejunum), kidney, brain, vaginal tissue, and rectal tissue were collected for quantitation of CAB and prodrug concentrations. CAB, MCAB, M2CAB, and M3CAB were quantitated in mouse plasma, blood, and tissues by UPLC-MS/MS using a Waters ACQUITY H-class UPLC (Waters, Milford, MA) connected to a Xevo TQ-S micro mass spectrometer. All solvents for sample processing and UPLC-MS/MS analysis were LC-MS-grade (Fisher). Detailed sample processing and quantitation methods are provided in supplementary methods. Non-compartmental PK analysis for plasma CAB in NSG mice was performed using Phoenix WinNonlin-8.0 software (Certara, Princeton, NJ). Toxicity in NSG mice was assessed by evaluating serum chemistry profiles and histological examination. For histological examination, 5 μm sections of paraffin-embedded tissues were stained with H&E. Images were captured with a 40× objective using a Nuance EX multispectral imaging system affixed to a Nikon Eclipse E800 microscope (Nikon Instruments, Melville, NY). Histopathological assessment was conducted by a certified pathologist in accordance with the guidelines of the Society of Toxicologic Pathology. Serum chemistry profiles were determined using a VetScan comprehensive diagnostic profile disc and a VetScan VS-2 instrument (Abaxis Veterinary Diagnostics, Union City, CA). Results for treated animals were compared to those from age-matched untreated control mice. PK and BD of NM2CAB were also evaluated in BALB/cJ mice (male, 6–8 weeks, Jackson Labs). NCAB was used as a control. Mice were dosed with NM2CAB (45 mg/kg CAB equivalents) by IM injection and were humanly euthanized at day 280 following treatment. Plasma and tissues were collected for drug and prodrug quantitation as described above for NSG mice. Drug-drug interactions between two prodrug nanoformulations, NM2CAB and NM3RPV, were evaluated in BALB/cJ mice (male, 6–8 weeks, Jackson Labs). Animals were treated IM with a single dose of NM2CAB alone (45 mg/kg CAB-equivalents), NM3RPV alone (45 mg/kg RPV-equivalents), or co-administration of both prodrug nanoformulations (NM2CAB and

NM3RPV, 45 mg/kg drug-equivalents for each). Plasma was collected up to day 49 for active drug (CAB and RPV) quantitation as described above for NSG mice.

PK and BD in rhesus macaques (RM)

For PK and BD studies in RM, NM2CAB was prepared in the Nebraska Nanomedicine Production Plant using good laboratory practices (GLP) protocols. The presuspension was prepared and homogenized as described above to form the final nanosuspension. Particle size, PDI, and zeta potential were determined by DLS (Malvern Zetasizer NanoZSP; Malvern Instruments). M2CAB concentration in the nanosuspension was determined by UPLC-MS/MS (Waters Acquity XevoTQ-S micro system; Waters Corp.) as described above. Endotoxin content was determined by the Lonza Limulus Amebocyte Lysate Pyrogent-500 test (Lonza, Walkersville, MD) and was found to be less than 5 EU/kg. Four male RM (4.4–6.7 kg; PrimeGen, Santa Ana, CA) were anesthetized with ketamine (10 mg/kg); each was administered 45 mg/kg CAB-equivalents of NM2CAB and a lab-generated RPV prodrug nanoformulation[16] by IM injection (quadriceps femoris muscle, 0.5 mL/kg). Blood samples were collected in potassium-EDTA coated tubes for complete blood counts (CBC), and plasma was isolated for metabolic profiles. Tissue biopsies of lymph nodes, adipose, and rectal tissues were collected at day 204 after injection for drug quantitation. Drug and prodrug in plasma and tissues were quantitated by UPLC-MS/MS as described for mouse samples.

Crystallization of M2CAB

Recrystallizations of 100 mg of M2CAB in 3.0 mL of ACN, MeTHF, CPME, or PhMe were carried out from solubilized prodrug solution at 65 °C. The solutions were then gradually cooled to 20 °C and stirred for 16 hours to form solid drug crystals that were consequently collected by filtration. Reproducibility of the recrystallization protocol was confirmed using 200 mg of M2CAB in ACN (4 mL). Chemical purity was measured by HPLC, and melting point of the solid samples were measured using capillary tubes in a Stuart SMP10 melting point apparatus (Vernon Hills, IL). The sample heating rate was 2 °C per minute. Physical appearance of the solids following recrystallization from ACN and CPME was assessed by XRD.

Statistical analyses

Statistical analyses were conducted using GraphPad Prism 7.0 software (La Jolla, CA). Data from *in vitro* studies were expressed as mean ± SEM with a minimum of three biological replicates. Results from *in vivo* studies were expressed as mean ± SEM with a minimum of three biological replicates. For comparisons between two groups, t test (two-tailed) with Welch's correction was used. A one-way ANOVA followed by Tukey's post-hoc test was used to compare three or more groups. Statistical significances were denoted as: *$P < 0.05$, **$P < 0.01$, ***$P < 0.001$, ****$P < 0.0001$. Linear regression models were used to examine the association between *in vitro* data and PK data.

Study approvals

All animal studies were approved by the University of Nebraska Medical Center Institutional Animal Care and Use Committee (IACUC) in accordance with the standards incorporated in the Guide for the Care and Use of Laboratory Animals (National Research Council of the National Academies, 2011). Human monocytes were isolated by leukapheresis from HIV-1/2 and hepatitis B seronegative donors according to an approved UNMC Institutional Review Board exempt protocol.

Supplementary Material

Refer to Web version on PubMed Central for supplementary material.

Acknowledgements

We thank the University of Nebraska Medical Center (UNMC) cores for NMR (Ed Ezell), Elutriation and Cell Separation (Myhanh Che, Na Ly, and Li Wu), Electron Microscopy (Nicholas Conoan and Tom Bargar), as well as Comparative Medicine for technical assistance and animal care. We also thank Dr. Shah Valloppilly of the University of Nebraska-Lincoln Nebraska Center for Materials and Nanoscience for X-Ray Structural Characterization. We thank Zhou You of the University of Nebraska-Lincoln Center for Biotechnology for SEM analysis of the nanoparticles. We also thank Dr. Alekha Dash and Daniel Munt of the Creighton University for the assistance in FTIR characterization and analysis. A special thank you to Dr. Samuel Cohen, UNMC, for the tissue histopathology assessments; and Dr. Prasanta K. Dash and Mr. Jonathan Herskovitz, UNMC, for grateful assistance in execution and interpretation of experiments used in these and related works. Ms. Robin Taylor, UNMC, is thanked for outstanding editorial support. This research is supported by the University of Nebraska Foundation, which includes donations from the Carol Swarts, M.D. Emerging Neuroscience Research Laboratory, the Margaret R. Larson Professorship, the Frances and Louie Blumkin Endowment, and the Harriet Singer Endowment; the Vice Chancellor's Office of the University of Nebraska Medical Center for Core Facilities; and the National Institutes of Health grants 1R01AI145542-01A1, P01 DA028555, R01 NS36126, P01 NS31492, 2R01 NS034239, P01 MH64570, P01 NS43985, P30 MH062261, R01 AG043540, and 1 R56 AI138613-01A1.

References

1. Fauci AS, Redfield RR, Sigounas G, Weahkee MD, Giroir BP. Ending the HIV Epidemic: A Plan for the United States. JAMA 2019, 321(9): 844–845. [PubMed: 30730529]
2. Gendelman HE, McMillan J, Bade AN, Edagwa B, Kevadiya BD. The Promise of Long-Acting Antiretroviral Therapies: From Need to Manufacture. Trends Microbiol 2019, 27(7): 593–606. [PubMed: 30981593]
3. Currier JS. Monthly Injectable Antiretroviral Therapy - Version 1.0 of a New Treatment Approach. N Engl J Med 2020.
4. Margolis DA, Gonzalez-Garcia J, Stellbrink HJ, Eron JJ, Yazdanpanah Y, Podzamczer D, et al. Long-acting intramuscular cabotegravir and rilpivirine in adults with HIV-1 infection (LATTE-2): 96-week results of a randomised, open-label, phase 2b, non-inferiority trial. Lancet 2017, 390(10101): 1499–1510. [PubMed: 28750935]
5. Orkin C, Arasteh K, Hernandez-Mora MG, Pokrovsky V, Overton ET, Girard PM, et al. Long-Acting Cabotegravir and Rilpivirine after Oral Induction for HIV-1 Infection. N Engl J Med 2020.
6. Swindells S, Andrade-Villanueva JF, Richmond GJ, Rizzardini G, Baumgarten A, Masia M, et al. Long-Acting Cabotegravir and Rilpivirine for Maintenance of HIV-1 Suppression. N Engl J Med 2020.
7. ViiV HEALTHCARE. ViiV HEALTHCARE SUBMITS NEW DRUG APPLICATION TO US FDA FOR THE FIRST MONTHLY, INJECTABLE, TWO-DRUG REGIMEN OF CABOTEGRAVIR AND RILPIVIRINE FOR TREATMENT OF HIV. 4 2019 [cited 2020 February 4th]Available from: https://viivhealthcare.com/en-gb/media/press-releases/2019/april/viiv-healthcare-submits-new-drug-application-to-us-fda-for-the-first-monthly-injectable-two-drug-regimen-of-cabotegravir-and-rilpivirine-for-treatment-of-hiv/

8. ViiV Healthcare. ViiV Healthcare receives complete response letter from US FDA for use of investigational cabotegravir and rilpivirine long-acting regimen in the treatment of HIV. 2019 [cited 2020 March 3]Available from: https://viivhealthcare.com/en-gb/media/press-releases/2019/december/complete-response-letter-from-us-fda/
9. Kovarova M, Benhabbour SR, Massud I, Spagnuolo RA, Skinner B, Baker CE, et al. Ultra-long-acting removable drug delivery system for HIV treatment and prevention. Nat Commun 2018, 9(1): 4156. [PubMed: 30297889]
10. Gunawardana M, Remedios-Chan M, Miller CS, Fanter R, Yang F, Marzinke MA, et al. Pharmacokinetics of long-acting tenofovir alafenamide (GS-7340) subdermal implant for HIV prophylaxis. Antimicrobial agents and chemotherapy 2015, 59(7): 3913–3919. [PubMed: 25896688]
11. Flexner C Antiretroviral implants for treatment and prevention of HIV infection. Current opinion in HIV and AIDS 2018, 13(4): 374–380. [PubMed: 29794816]
12. Barrett SE, Teller RS, Forster SP, Li L, Mackey MA, Skomski D, et al. Extended-Duration MK-8591-Eluting Implant as a Candidate for HIV Treatment and Prevention. Antimicrobial agents and chemotherapy 2018, 62(10).
13. Markowitz M, Frank I, Grant RM, Mayer KH, Elion R, Goldstein D, et al. Safety and tolerability of long-acting cabotegravir injections in HIV-uninfected men (ECLAIR): a multicentre, double-blind, randomised, placebo-controlled, phase 2a trial. Lancet HIV 2017, 4(8): e331–e340. [PubMed: 28546090]
14. Zhou T, Su H, Dash P, Lin Z, Dyavar Shetty BL, Kocher T, et al. Creation of a nanoformulated cabotegravir prodrug with improved antiretroviral profiles. Biomaterials 2018, 151: 53–65. [PubMed: 29059541]
15. Dash PK, Kaminski R, Bella R, Su H, Mathews S, Ahooyi TM, et al. Sequential LASER ART and CRISPR Treatments Eliminate HIV-1 in a Subset of Infected Humanized Mice. Nat Commun 2019, 10(1): 2753. [PubMed: 31266936]
16. Hilaire JR, Bade AN, Sillman B, Gautam N, Herskovitz J, Dyavar Shetty BL, et al. Creation of a long-acting rilpivirine prodrug nanoformulation. J Control Release 2019, 311–312: 201–211.
17. Sillman B, Bade AN, Dash PK, Bhargavan B, Kocher T, Mathews S, et al. Creation of a long-acting nanoformulated dolutegravir. Nat Commun 2018, 9(1): 443. [PubMed: 29402886]
18. Smith N, Bade AN, Soni D, Gautam N, Alnouti Y, Herskovitz J, et al. A long acting nanoformulated lamivudine ProTide. Biomaterials 2019, 223: 119476. [PubMed: 31525692]
19. Soni D, Bade AN, Gautam N, Herskovitz J, Ibrahim IM, Smith N, et al. Synthesis of a long acting nanoformulated emtricitabine ProTide. Biomaterials 2019, 222: 119441. [PubMed: 31472458]
20. Huttunen KM, Raunio H, Rautio J. Prodrugs--from serendipity to rational design. Pharmacol Rev 2011, 63(3): 750–771. [PubMed: 21737530]
21. Rautio J, Kumpulainen H, Heimbach T, Oliyai R, Oh D, Jarvinen T, et al. Prodrugs: design and clinical applications. Nat Rev Drug Discov 2008, 7(3): 255–270. [PubMed: 18219308]
22. Bahar FG, Ohura K, Ogihara T, Imai T. Species difference of esterase expression and hydrolase activity in plasma. Journal of pharmaceutical sciences 2012, 101(10): 3979–3988. [PubMed: 22833171]
23. Malamatari M, Taylor KMG, Malamataris S, Douroumis D, Kachrimanis K. Pharmaceutical nanocrystals: production by wet milling and applications. Drug Discov Today 2018, 23(3): 534–547. [PubMed: 29326082]
24. Zhou T, Lin Z, Puligujja P, Palandri D, Hilaire J, Arainga M, et al. Optimizing the preparation and stability of decorated antiretroviral drug nanocrystals. Nanomedicine (Lond) 2018, 13(8): 871–885. [PubMed: 29553879]
25. Darville N, van Heerden M, Vynckier A, De Meulder M, Sterkens P, Annaert P, et al. Intramuscular administration of paliperidone palmitate extended-release injectable microsuspension induces a subclinical inflammatory reaction modulating the pharmacokinetics in rats. Journal of pharmaceutical sciences 2014, 103(7): 2072–2087. [PubMed: 24845884]
26. Kadiu I, Nowacek A, McMillan J, Gendelman HE. Macrophage endocytic trafficking of antiretroviral nanoparticles. Nanomedicine (Lond) 2011, 6(6): 975–994. [PubMed: 21417829]

27. Nowacek A, Kadiu I, McMillan J, Gendelman HE. Immunoisolation of nanoparticles containing endocytic vesicles for drug quantitation. Methods Mol Biol 2013, 991: 41–46. [PubMed: 23546657]
28. McMillan J, Szlachetka A, Slack L, Sillman B, Lamberty B, Morsey B, et al. Pharmacokinetics of a Long-Acting Nanoformulated Dolutegravir Prodrug in Rhesus Macaques. Antimicrobial agents and chemotherapy 2018, 62(1).
29. Rohani S, Horne S, Murthy K. Control of Product Quality in Batch Crystallization of Pharmaceuticals and Fine Chemicals. Part 1: Design of the Crystallization Process and the Effect of Solvent. Organic Process Research & Development 2005, 9(6): 858–872.
30. Nair AB, Jacob S. A simple practice guide for dose conversion between animals and human. J Basic Clin Pharm 2016, 7(2): 27–31. [PubMed: 27057123]
31. Kerrigan D, Mantsios A, Gorgolas M, Montes ML, Pulido F, Brinson C, et al. Experiences with long acting injectable ART: A qualitative study among PLHIV participating in a Phase II study of cabotegravir + rilpivirine (LATTE-2) in the United States and Spain. PloS one 2018, 13(1): e0190487. [PubMed: 29304154]
32. Osterberg L, Blaschke T. Adherence to medication. N Engl J Med 2005, 353(5): 487–497. [PubMed: 16079372]
33. Shubber Z, Mills EJ, Nachega JB, Vreeman R, Freitas M, Bock P, et al. Patient-Reported Barriers to Adherence to Antiretroviral Therapy: A Systematic Review and Meta-Analysis. PLoS medicine 2016, 13(11): e1002183. [PubMed: 27898679]
34. Edagwa B, McMillan J, Sillman B, Gendelman HE. Long-acting slow effective release antiretroviral therapy. Expert opinion on drug delivery 2017, 14(11): 1281–1291. [PubMed: 28128004]
35. Trezza C, Ford SL, Spreen W, Pan R, Piscitelli S. Formulation and pharmacology of long-acting cabotegravir. Current opinion in HIV and AIDS 2015, 10(4): 239–245. [PubMed: 26049948]
36. Wang D, Zou L, Jin Q, Hou J, Ge G, Yang L. Human carboxylesterases: a comprehensive review. Acta pharmaceutica Sinica B 2018, 8(5): 699–712. [PubMed: 30245959]
37. McPherson TD, Sobieszczyk ME, Markowitz M. Cabotegravir in the treatment and prevention of Human Immunodeficiency Virus-1. Expert Opin Investig Drugs 2018, 27(4): 413–420.
38. Stellbrink HJ, Hoffmann C. Cabotegravir: its potential for antiretroviral therapy and preexposure prophylaxis. Current opinion in HIV and AIDS 2018, 13(4): 334–340. [PubMed: 29746267]
39. Rautio J, Meanwell NA, Di L, Hageman MJ. The expanding role of prodrugs in contemporary drug design and development. Nat Rev Drug Discov 2018, 17(8): 559–587. [PubMed: 29700501]
40. Landovitz RJ, Li S, Grinsztejn B, Dawood H, Liu AY, Magnus M, et al. Safety, tolerability, and pharmacokinetics of long-acting injectable cabotegravir in low-risk HIV-uninfected individuals: HPTN 077, a phase 2a randomized controlled trial. PLoS medicine 2018, 15(11): e1002690. [PubMed: 30408115]
41. Murray MI, Markowitz M, Frank I, Grant RM, Mayer KH, Hudson KJ, et al. Satisfaction and acceptability of cabotegravir long-acting injectable suspension for prevention of HIV: Patient perspectives from the ECLAIR trial. HIV Clin Trials 2018, 19(4): 129–138. [PubMed: 30445896]
42. Penrose KJ, Parikh UM, Hamanishi KA, Else L, Back D, Boffito M, et al. Selection of Rilpivirine-Resistant HIV-1 in a Seroconverter From the SSAT 040 Trial Who Received the 300-mg Dose of Long-Acting Rilpivirine (TMC278LA). J Infect Dis 2016, 213(6): 1013–1017. [PubMed: 26563240]
43. Bollinger RC, Thio CL, Sulkowski MS, McKenzie-White J, Thomas DL, Flexner C. Addressing the global burden of hepatitis B virus while developing long-acting injectables for the prevention and treatment of HIV. Lancet HIV 2019.
44. Ford SL, Sutton K, Lou Y, Zhang Z, Tenorio A, Trezza C, et al. Effect of Rifampin on the Single-Dose Pharmacokinetics of Oral Cabotegravir in Healthy Subjects. Antimicrobial agents and chemotherapy 2017, 61(10).
45. Rajoli RKR, Curley P, Chiong J, Back D, Flexner C, Owen A, et al. Predicting Drug-Drug Interactions Between Rifampicin and Long-Acting Cabotegravir and Rilpivirine Using Physiologically Based Pharmacokinetic Modeling. J Infect Dis 2019, 219(11): 1735–1742. [PubMed: 30566691]

46. National Institute of Allergy and Infectious Diseases (NIAID). Experimental HIV vaccine regimen ineffective in preventing HIV. 2020 [cited 2020 February 7]Available from: https://www.nih.gov/news-events/news-releases/experimental-hiv-vaccine-regimen-ineffective-preventing-hiv

47. Benitez-Gutierrez L, Soriano V, Requena S, Arias A, Barreiro P, de Mendoza C. Treatment and prevention of HIV infection with long-acting antiretrovirals. Expert Rev Clin Pharmacol 2018, 11(5): 507–517. [PubMed: 29595351]

48. de Mendoza C, Soriano V. Tough requirements for new antiretroviral drugs. Lancet HIV 2020.

49. Smith RA, Wu VH, Zavala CG, Raugi DN, Ba S, Seydi M, et al. In Vitro Antiviral Activity of Cabotegravir against HIV-2. Antimicrobial agents and chemotherapy 2018, 62(10).

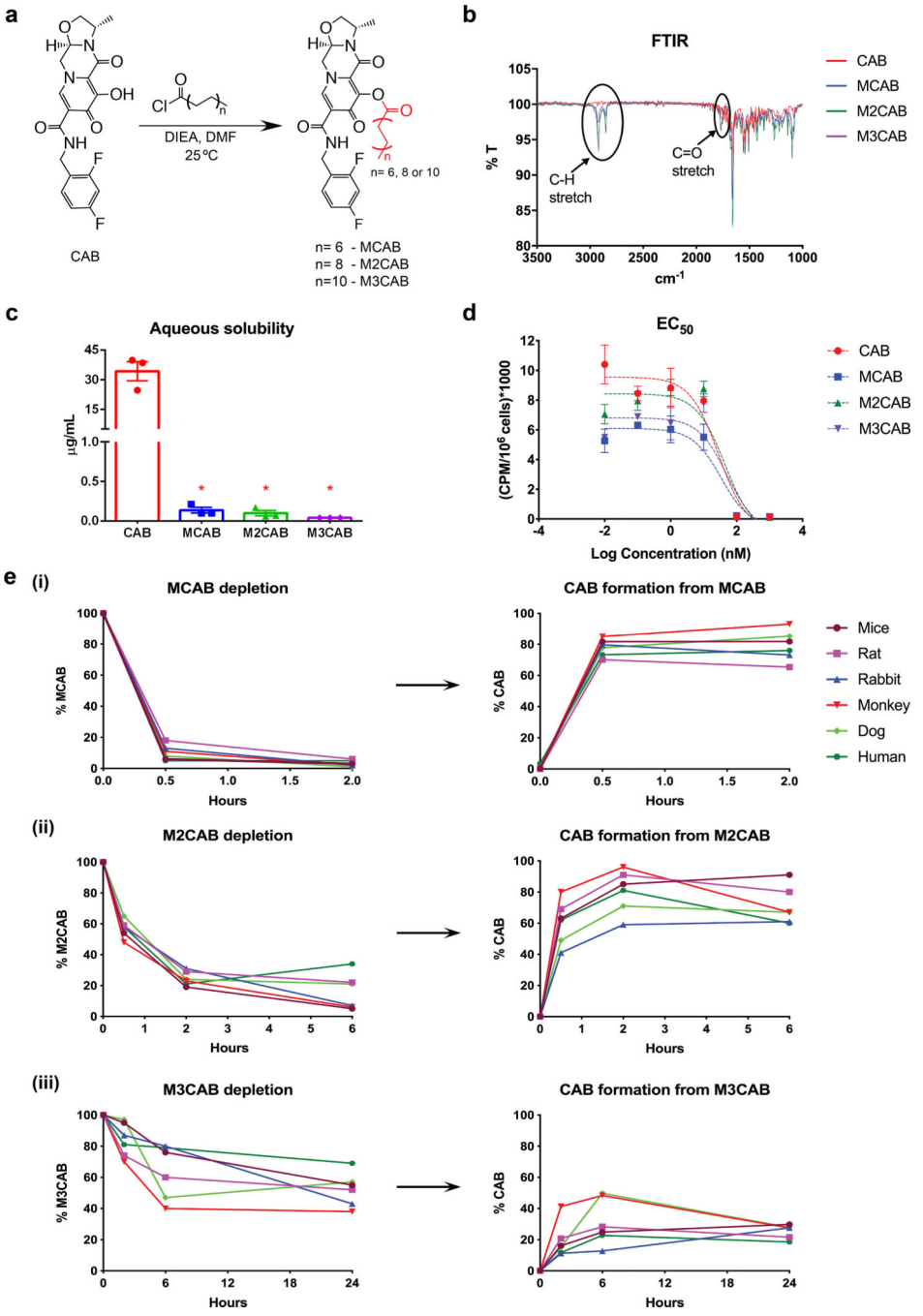

Figure 1. Synthesis and characterization of CAB prodrugs.

(**a**) CAB was chemically modified with 14, 18, and 22 carbon fatty acid chains to develop MCAB, M2CAB, and M3CAB, respectively. (**b**) FTIR spectra show the presence of absorption bands around 2,919 cm^{-1} and 1,765 cm^{-1} corresponding to C-H stretch in fatty acid methylene groups and carbonyl stretch, respectively. Data was independently reproduced three times. (**c**) Aqueous solubility of CAB and prodrugs. Data are expressed as the mean ± SEM for N = 3 (CAB), 3 (NMCAB), 3 (NM2CAB), and 3 (NM3CAB) biologically independent samples. t test (two-tailed) with Welch's correction was used to

compare the solubility between CAB and individual prodrug. (*P < 0.05). (**d**) Antiviral activity was determined in MDM over a range of concentrations (0.01 – 1,000 nM) by measuring HIV-1 RT activity after challenge with HIV-1_{ADA} at an MOI of 0.1. Data are expressed as the mean ± SEM for N = 3 biological replicates. (**e**) Plasma cleavage kinetics. Bioconversion of prodrugs into active CAB in plasma of various species (mice, rat, rabbit, monkey, dog, and human) was assessed. Experiments were repeated independently two times with equivalent results.

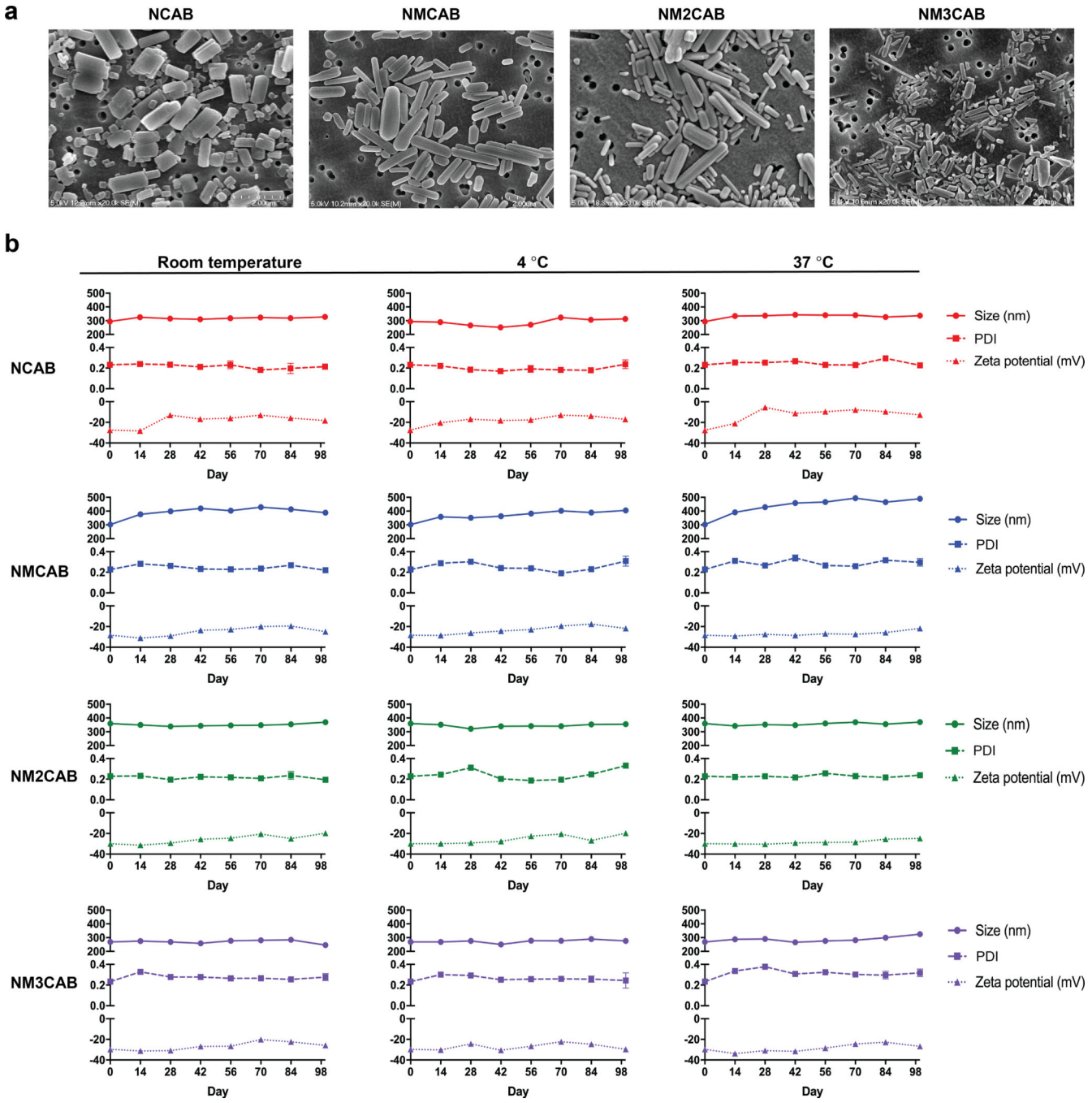

Figure 2. Synthesis and characterization of nanoformulations of CAB and prodrugs.

(**a**) Morphological assessment of NCAB, NMCAB, NM2CAB, and NM3CAB by SEM. Data was independently reproduced three times. (**b**) The stability of CAB and prodrug nanoformulations was evaluated over 98 days following manufacture at room temperature, 4 ºC, and 37 ºC as determined by size (nm), polydispersity index (PDI), and zeta potential (mV). Data are expressed as the mean ± SEM for N = 3 biological replicates.

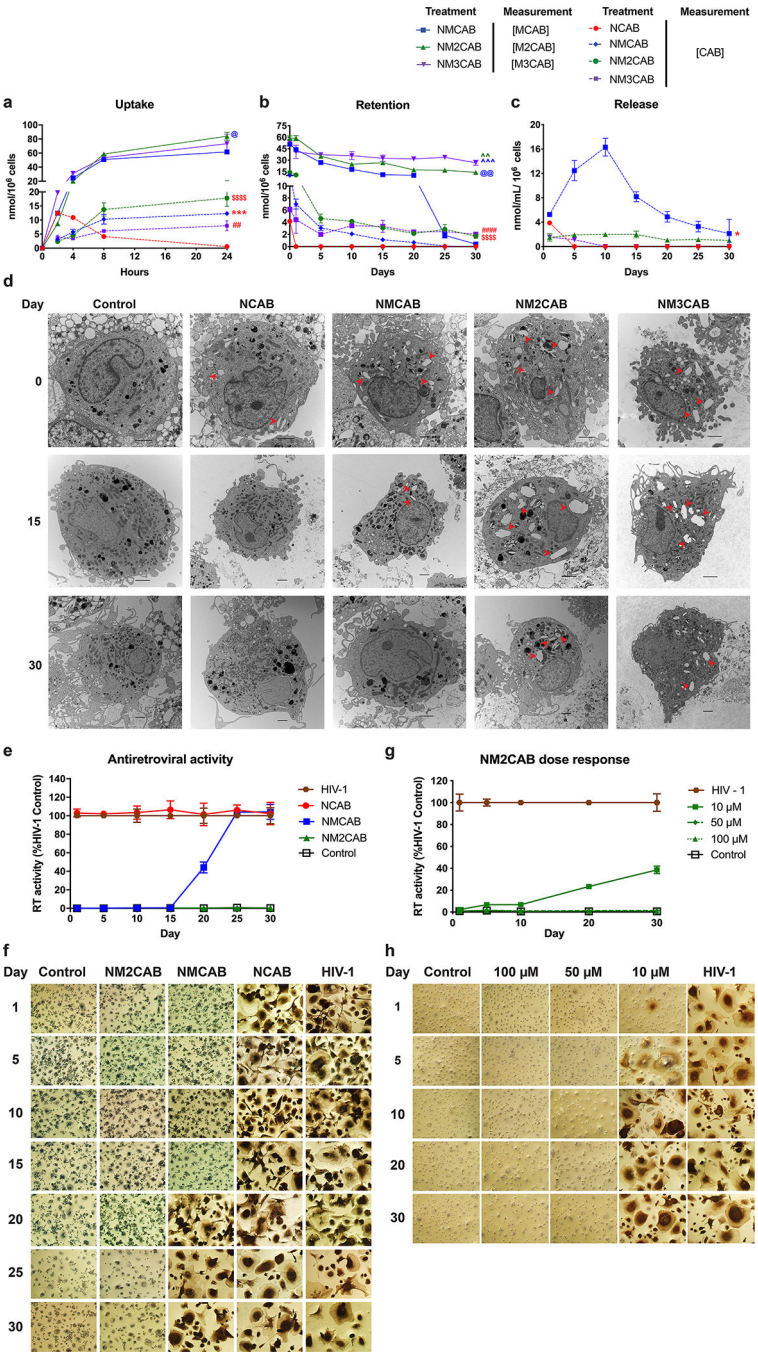

Figure 3. ***In vitro*** **characterization.**

(**a**) Cellular uptake and (**b**) retention of drug and each prodrug in MDM was assessed. (**c**) In parallel, CAB released into the culture medium was measured. For uptake study, a one-way ANOVA followed by Tukey's post-hoc test was used to compare CAB levels among four treatment groups (red colored $^{\#\#}P < 0.01$, $^{***}P < 0.001$, $^{\$\$\$\$}P < 0.0001$ compared to NCAB), and prodrug levels among three treatment groups (blue colored $^{@}P < 0.05$ compared NMCAB). For retention study, a one-way ANOVA followed by Tukey post-hoc test was used to compare CAB levels among four treatment groups (red colored $^{\$\$\$\$}P <$

0.0001, ####P < 0.0001 compared to NCAB), and prodrug levels among three treatment groups (blue colored @@P < 0.01, ^^^P < 0.001 compared to NMCAB, and green colored ^^P < 0.01 compared to NM2CAB). For release study, a one-way ANOVA followed by Tukey's post-hoc test was used to compare CAB levels among four treatment groups (red colored *P < 0.05). For all assays, data are expressed as mean ± SEM, N = 3 biological replicates. (**d**) TEM images of MDM treated with each nanoformulation and of untreated control. Red arrowheads indicate nanocrystals present in the cytoplasm. Scale bars = 2 μm. Data was independently reproduced three times. (**e**) Antiretroviral activity. Infection was determined by measuring HIV-1 RT activity in culture medium; and (**f**) HIV-1 p24 antigen immunocytochemistry. (**g and h**) The antiretroviral concentration-response of NM2CAB. (**e and g**) HIV-1 RT activity was expressed as mean ± SEM, N = 4 biological replicates. (**f and h**) Each experiment was repeated independently three times with equivalent results.

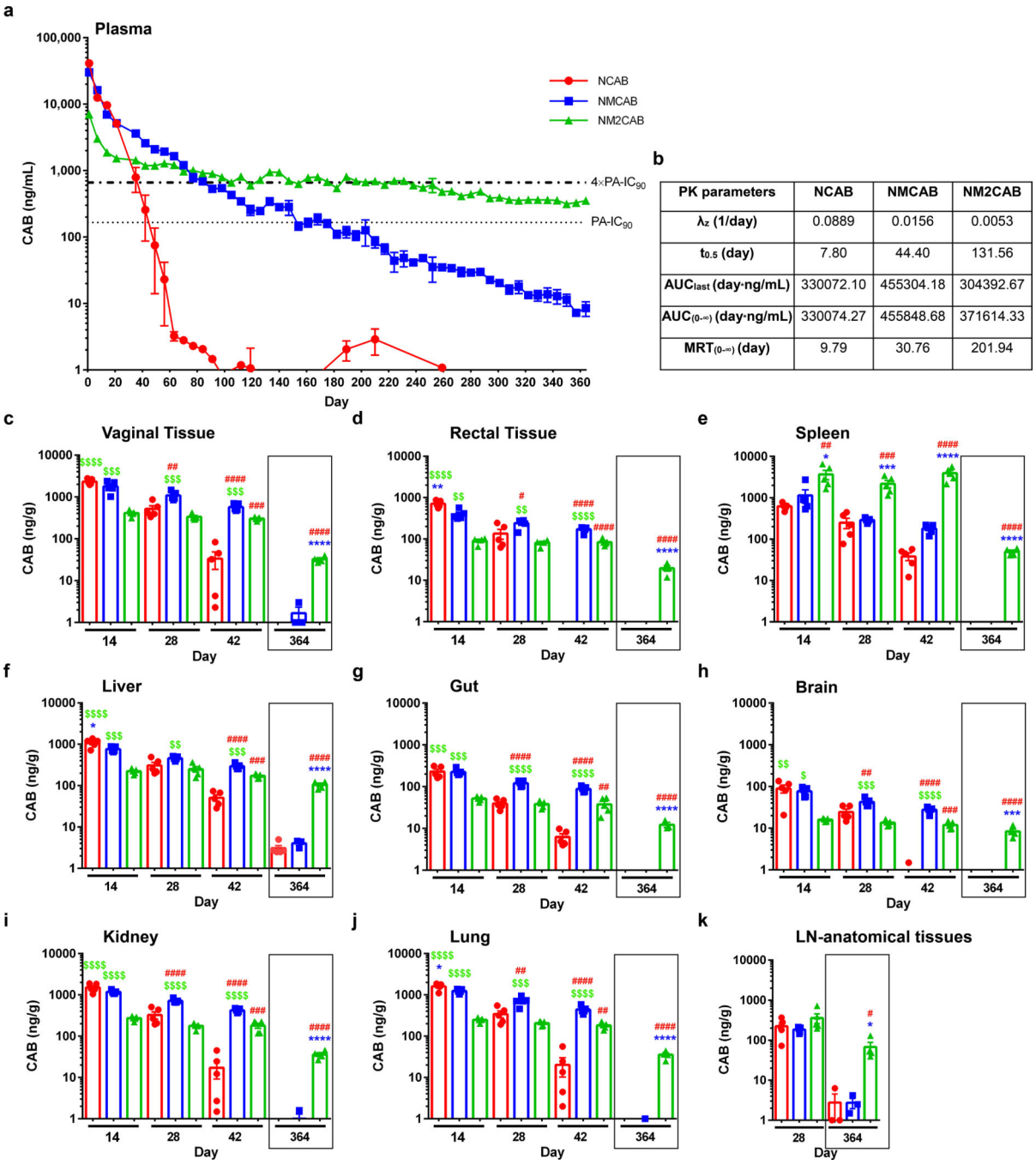

PK parameters	NCAB	NMCAB	NM2CAB
λ_z (1/day)	0.0889	0.0156	0.0053
$t_{0.5}$ (day)	7.80	44.40	131.56
AUC_{last} (day·ng/mL)	330072.10	455304.18	304392.67
$AUC_{(0-\infty)}$ (day·ng/mL)	330074.27	455848.68	371614.33
$MRT_{(0-\infty)}$ (day)	9.79	30.76	201.94

Figure 4. CAB levels in plasma and tissues.

(**a**) Plasma drug levels in NSG mice. Top bold dashed line indicates plasma CAB 4×PA-IC_{90} (664 ng/mL), and bottom stippled line shows the plasma CAB 1×PA-IC_{90} (166 ng/mL). Data are expressed as mean ± SEM. Study was initiated with N = 5 animals per group. Due to loss of animals by natural causes during study period, animals at day 364, N = 5 (NCAB), N = 3 (NMCAB), and N = 4 (NM2CAB). (**b**) Plasma pharmacokinetic parameters for CAB were determined using non-compartmental analyses. λ_Z, (individual estimate of the terminal elimination rate constant); $t_{0.5}$ (half-life); $AUC_{0-\infty}$ (area under the plasma concentration

time curve (AUC) from 0 hour to infinity); AUC_{last} (AUC 0 hour to last time point); MRT (mean residence time). (**c-k**) Tissue biodistribution of CAB was assessed at days 14, 28, 42, and 364 in (**c**) vaginal tissue, (**d**) rectal tissue, (**e**) spleen, (**f**) liver, (**g**) gut, (**h**) brain, (**i**) kidney, (**j**) lung, and (**k**) lymph nodes-anatomical associated tissues. Drug levels in lymph nodes (k) were determined in anatomical regions associated with lymph nodes only at day 28 and 364, due to their immature state in immunodeficient NSG mice. (**c-k**) Data are expressed as mean ± SEM. For days 14, 28, and 42 groups, N = 5 animals/group, and for the day 364, N = 5 (NCAB), N = 3 (NMCAB), and N = 4 (NM2CAB) animals. A one-way ANOVA followed by Tukey's post-hoc test was used to compare drug levels in tissues among three treatments ($^{\#}P < 0.05$, $^{\#\#}P < 0.01$, $^{\#\#\#}P < 0.001$, $^{\#\#\#\#}P < 0.0001$ compared to NCAB; $^{*}P < 0.05$, $^{**}P < 0.01$, $^{***}P < 0.001$, $^{****}P < 0.0001$ compared to NMCAB; $^{\$}P < 0.05$, $^{\$\$}P < 0.01$, $^{\$\$\$}P < 0.001$, $^{\$\$\$\$}P < 0.0001$ compared to NM2CAB).

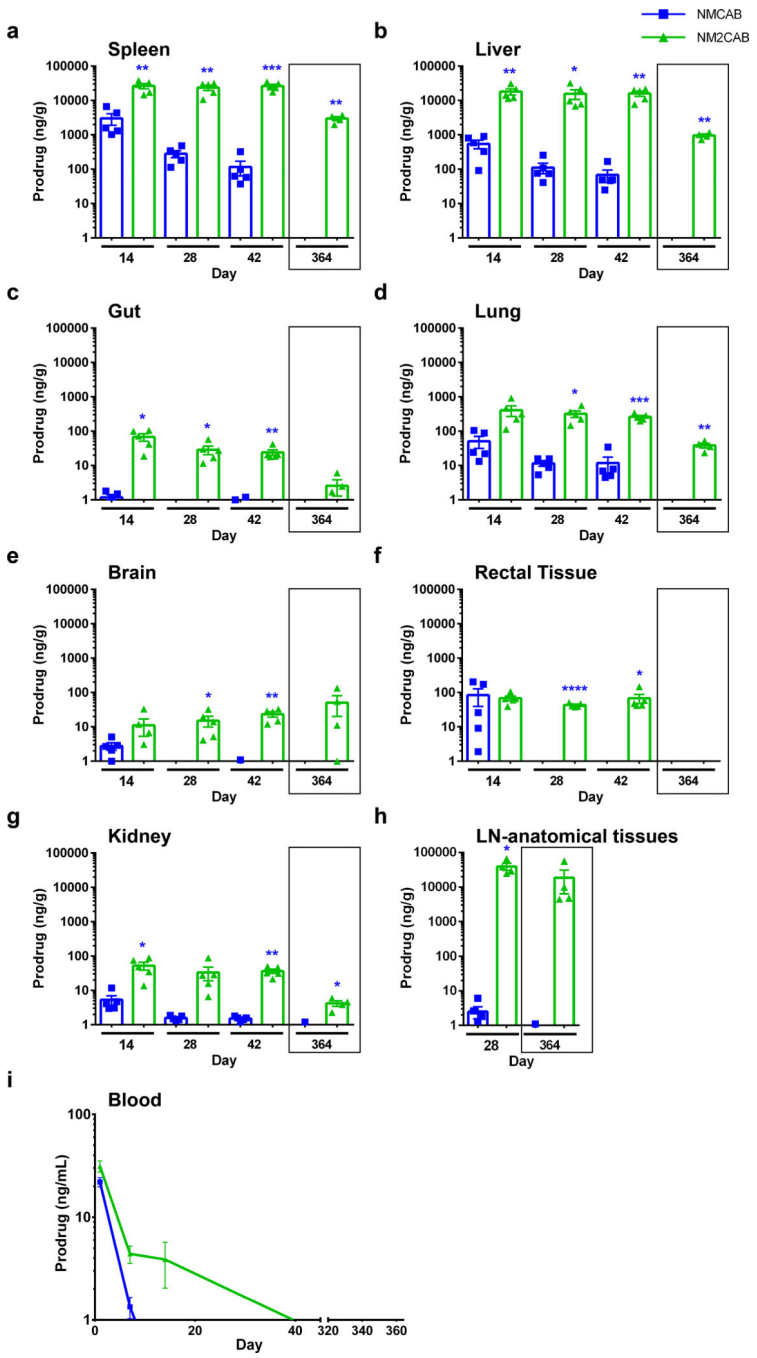

Figure 5. Prodrug measurements.

Tissue and blood concentrations of prodrugs (MCAB or M2CAB) were determined at 14, 28, 42 and 364 days after a single IM injection of NMCAB or NM2CAB. Prodrug levels were measured in the (**a**) spleen, (**b**) liver, (**c**) gut, (**d**) lung, (**e**) brain, (**f**) rectal tissue, (**g**) kidneys, (**h**) lymph nodes-anatomical associated tissues, and (**i**) blood. Prodrug levels in lymph nodes were determined in anatomical regions associated with lymph nodes only at days 28 and 364, due to their immature state in immunodeficient NSG mice. (**a-h**) Data are expressed as mean ± SEM. For days 14, 28, and 42 groups, animal numbers in each group

were N = 5, and for the day 364 group animal numbers were N = 3 (NMCAB), and N = 4 (NM2CAB). t test (two-tailed) with Welch's correction was used to compare prodrug levels in tissues at the respective time points (*P < 0.05, **P < 0.01, ***P < 0.001, ****P < 0.0001). (**i**) Data are expressed as mean ± SEM. Study was initiated with N = 5 animals in each group (NCAB, NMCAB or NM2CAB). Due to loss of animals by natural causes during study period, by the day 364 post-treatment, N = 5 (NCAB), N = 3 (NMCAB) and N = 4 (NM2CAB) animals.

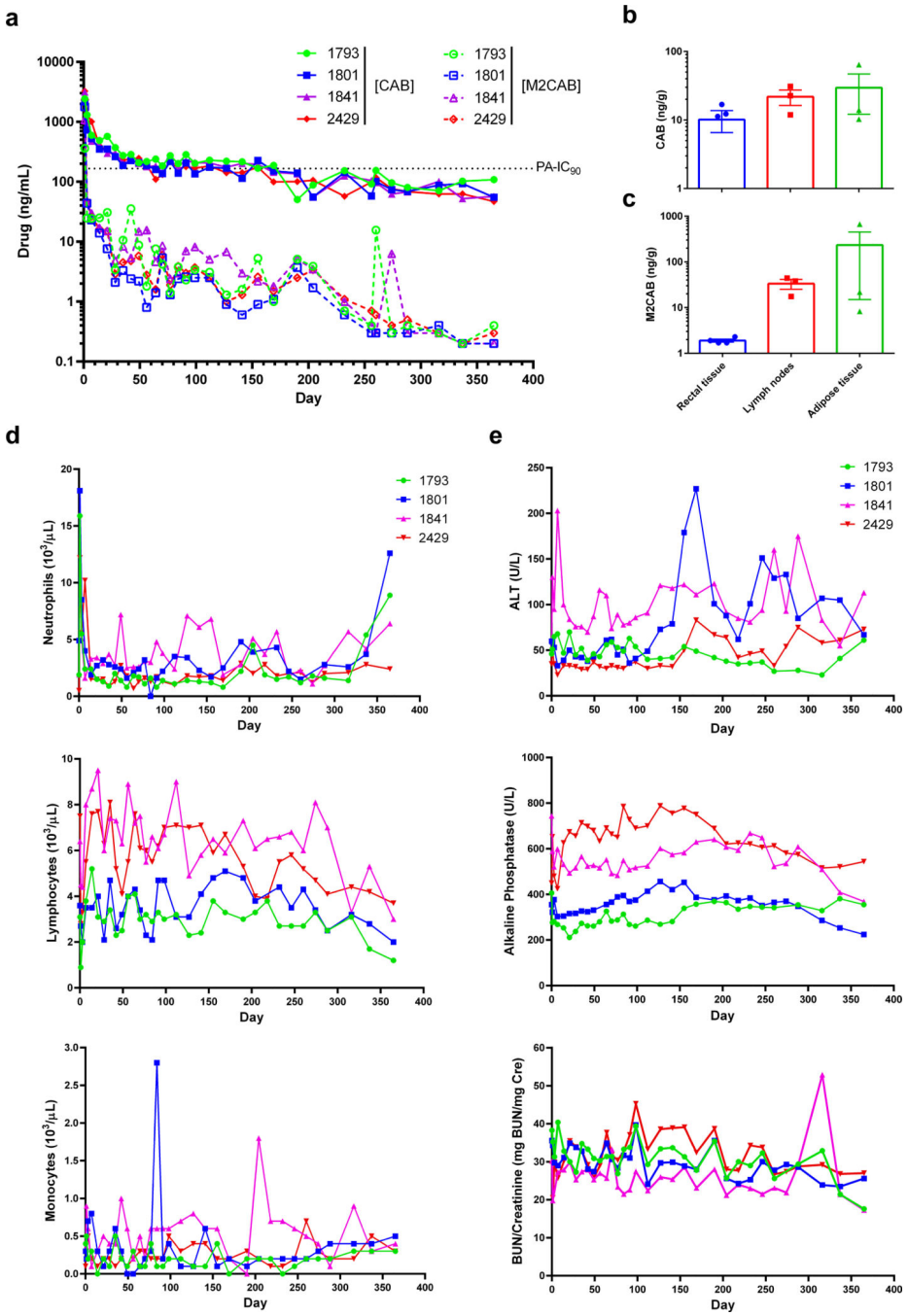

Figure 6. PK, BD, and toxicological assessments in rhesus macaques.

Four rhesus macaques were administered a 45 mg/kg CAB-equivalent dose of NM2CAB by a single IM injection. (**a**) Plasma samples were collected, and CAB and M2CAB levels were determined up to day 365. (**b and c**) Rectal, lymph node, and adipose tissue biopsies were collected at day 204 following drug administration and assayed for (**b**) CAB and (**c**) M2CAB concentrations. (**d and e**) Systemic adverse reactions were evaluated by measuring (**d**) hematologic and (**e**) metabolic profiles. Plasma drug and prodrug concentrations, and

hematologic and metabolic profile parameters are shown for individual animals. Tissue drug concentrations are expressed as mean ± SEM; N = 4 animals.